Vibrationally resolved inelastic scattering and charge transfer in H+ +C2H2 collisions

Natasha Aristov, Gereon NiednerSchatteburg, J. Peter Toennies, and YingNan Chiu

Citation: The Journal of Chemical Physics **95**, 7969 (1991); doi: 10.1063/1.461328
View online: http://dx.doi.org/10.1063/1.461328
View Table of Contents: http://scitation.aip.org/content/aip/journal/jcp/95/11?ver=pdfcov
Published by the AIP Publishing

Vibrationally resolved inelastic scattering and charge transfer in $H^+ + C_2H_2$ collisions

Natasha Aristov,[a)] Gereon Niedner-Schatteburg,[b)] J. Peter Toennies
Max-Planck-Institut für Strömungsforschung, Bunsenstrasse 10, D-3400 Göttingen, Germany

Ying-Nan Chiu
Center for Molecular Dynamics and Energy Transfer, Department of Chemistry, The Catholic University of America, Washington, D.C. 20064

(Received 4 February 1991; accepted 23 April 1991)

Differential total cross sections and time-of-flight spectra for inelastic scattering and charge transfer of protons with acetylene have been measured in a crossed molecular beam apparatus at 30 eV collision energy. Both vibrational excitation of the C–C stretch and C–H stretch vibrations are resolved in the time-of-flight spectra. The angular distributions indicate the existence of a potential well in the entrance channel of 1.2 eV. The angle dependence of the time-of-flight spectra reveal that the stiff C–H stretch vibrations are preferentially excited in grazing collisions by long range electrostatic multipole interactions, whereas the C–C stretch vibrations although softer are only excited by a short range interaction. The vibrational normal modes observed to be excited can be explained in terms of a proposed potential hypersurface and the associated nonadiabatic couplings and vibronic symmetry correlations.

I. INTRODUCTION

Protons are unique scattering particles for studying ion-molecule interactions. Since they are structureless they cannot themselves undergo inelastic transitions. Because of their light mass the collision times are short and inelastic processes are highly probable. The small mass of the proton simplifies the kinematical interpretation of angular distributions and enhances the energy loss resolution of inelastic events in scattering experiments. Because of their simplicity, the interaction of protons with molecules is especially amenable to theoretical treatment. These systems are also of great practical interest for understanding flames, plasmas, upper atmosphere reactions, and astrophysical phenomena.

The present study of the high resolution inelastic scattering of protons from C_2H_2 is part of an ongoing study of proton interactions with simple organic molecules. In the first of this series we reported on results for CH_4 (Ref. 1) which were discussed using symmetry arguments. In forthcoming publications we will deal with C_2H_4 and C_6H_6.

In the apparatus a nearly monoenergetic beam of 30 eV protons is scattered from a nozzle beam of the target molecules. The time-of-flight and angular distributions of the protons as well as of H atoms formed by charge transfer are measured by an open electron multiplier detector. In the first demonstration of this technique for studying charge transfer, the vibrational state distribution of the O_2^+ ions produced in the $H^+ + O_2 \rightarrow H + O_2^+$ reaction was determined.[2] Stückelberg oscillations[3] are observed when krypton and xenon are used as the targets.[4] Such oscillations are due to interferences between different elastic and charge transfer pathways. The experimental results for the rare gases are nicely reproduced by quantum mechanical calculations.[4] When protons collide with hydrogen molecules the charge transfer process is highly endoergic. It is strongly promoted through H_2 vibrational excitation and is found to proceed in a two-step mechanism.[5] The experimental results are modeled rather well by quantum mechanical calculations[6,7] whereas a semiclassical description is somewhat less successful.[5] In contrast to the behavior of H_2, the charge transfer and vibrational excitation channels in collisions of $H^+ + CO_2$ or $H^+ + N_2O$ are largely decoupled.[8] Charge transfer in $H^+ + H_2O$ populates two electronic states of H_2O^+.[9] The vibrational distributions in these states deviate significantly from those prepared by photoionization. This has been explained by the propensity for charge transfer excitation of those vibrations of the molecular ions states for which the overall energy transfer is minimized.

In addition to studying the state to state dynamics, the chemical aspects have also been examined. Increased fluorination of methane leads to increased energy transfer.[10,11] For $H + CF_4$ only inelastic excitations are observed. For this system the inelastic scattering time-of-flight spectra have the greatest resolution[12] and very high overtones, up to $n = 14$, can be excited. Further work is in progress on CF_4 in a new apparatus with much greater energy resolution.[13]

In small angle collisions a long-range induced dipole mechanism (IDM) is important[14] in most of the molecules studied so far. In the previously mentioned $H^+ + CH_4$ system,[1] two additional possible vibrational excitation mechanisms were also discussed: an internal vibronic mechanism (IVM) and a close-range quasimolecular mechanism (QMM). Each mechanism leads to the excitation of different normal modes with different distributions. The analysis of the CH_4 experiments is especially challenging because the Jahn–Teller distortion in the methane cation[15] breaks the degeneracy of several vibrational modes and allows additional transitions to occur.

[a)] Present address: Springer Verlag, Tiergartenstr. 17, D-6900 Heidelberg 1, Germany.
[b)] Present address: Institut für Physikalische und Theoretische Chemie, Technische Universität München, D-8046 Garching, Germany.

In this article we investigate the two competing processes of inelastic scattering

$$H^+ + C_2H_2(\nu_i) \rightarrow H^+ + C_2H_2(\nu_f) \quad (1)$$

and charge transfer

$$H^+ + C_2H_2(\nu_i) \rightarrow H + C_2H_2^+(\nu_f), \quad (2)$$

where ν_i and ν_f are the initial and final vibrational levels of a particular normal mode of the acetylene molecule or molecular ion. For later reference we denote process (1) as "inelastic scattering" (IS) and process (2) as "charge transfer" (CT), although vibrational excitation of the molecular ion will also be present. The motions, symmetries, and energies of the normal modes of C_2H_2 and $C_2H_2^+$ are tabulated in Table I. In addition, for later discussion the same information is presented for two structures of the $C_2H_3^+$ complex. Figure 1 shows the energy levels of the fundamentals and most of the overtones and combinations present up to total internal energies of 0.7 eV.

This article is organized as follows: The apparatus is briefly described first. The relative angular distributions and the energy loss spectra for inelastic scattering and energy transfer are presented. From these data vibrational transition probabilities and average internal energy transfer are calculated and compared for C_2H_2 and $C_2H_2^+$. The dynamical theory is discussed and the important coupling matrix elements are identified for the three mechanisms IDM, IVM, and QMM. A potential hypersurface has been constructed from available quantum chemical calculations and used to explain the important scattering features. The possible allowed vibrational normal mode excitations are obtained for the three mechanisms and compared with the experiments.

II. APPARATUS

The apparatus is essentially the same as described previously.[2,4,12] Briefly, a mass- and energy-selected pulsed proton beam crosses an effusive, uncollimated target molecular beam. The entire proton source is rotated in a plane perpendicular to the secondary beam inside the vacuum chamber. The inelastically scattered protons or H atoms produced in charge transfer collisions are detected as a function of the flight time at the end of a 2.93 m long flight tube by the same particle multiplier. When measuring the H-atom signal, the protons are suppressed by a 200 V repelling field applied to a ring electrode inside the flight tube. The detection efficiency of 30 eV H atoms is estimated to be $5 \pm 2\%$.[4] Since the protons are accelerated by the 3 kV field of the multiplier their detection efficiency is nearly 100%. The signal intensity varies from $10^3\ s^{-1}$ when counting protons at small angles to less than one detected event per minute when counting H atoms at large angles. In order to have both good time-of-flight resolution ($\sim E^{-1/2}$) and high detection efficiency for neutral H atoms $\sim [1 - \exp(-aE)]$,[20] the present experiments are restricted to a narrow range of collision energies near 30 eV.

TABLE I. Symmetries and energies of vibrational modes of C_2H_2, $C_2H_2^+$, and $C_2H_3^+$.[a]

	$C_2H_2(D_{\infty h})$[b]		$C_2H_2^+(D_{\infty h})$[d]			$C_2H_3^+(C_{2v}^x)$[e] (non-classical)		$C_2H_3^+(C_{2v}^z)$[e] (classical)	
Mode	Symmetry	Energy	Symmetry	Energy	Mode	Symmetry	Energy	Symmetry	Energy
C–H *s* stretch	(ν_1) σ_g^+	418 (0)[c]	σ_g^+	407	C–H *s* stretch	a_1	404	a_1	393
					Bridge C–H stretch	a_1	312		
C–C stretch	(ν_2) σ_g^+	245 (0)	σ_g^+	227	C–C stretch	a_1	235	a_1	201
C–H *a* stretch	(ν_3) σ_u^+	408 (1.04)		389[h]	C–H *a* stretch	b_1	390		
					Bridging C–H bend				
C–H *s* bend[f]	(ν_4) π_{gx}	76 (0)		62	Out-of-plane	a_2	73	b_2	57
	π_{gy}	76 (0)		···	In-plane	b_1	164		
C–H *a* bend[f]	(ν_5) π_{ux}	90 (1.17)		87	C–H bend				
	π_{uy}	90 (1.17)		38	Out-of-plane	b_2	89		
					In-plane	a_1	123	b_1	83
					Ring deformation	b_1	47		
					CH_2 scissor			a_1	169
					CH_2 *a* stretch			b_1	376
					CH_2 *s* stretch			a_1	366
					CH_2 wag in-plane[g]			b_1	145
					CH_2 rock out-of-plane[g]			b_2	128

[a] Energies in meV.
[b] Reference 15.
[c] Numbers in parentheses are derivatives of the dipole moment (in units of 10^{-6} A s kg$^{-1/2}$) (Ref. 16).
[d] Reference 17.
[e] Calculated and estimated from Refs. 18 and 19.
[f] There is some discrepancy in the literature as to the geometry of these modes. We use Herzberg's definition (Ref. 15): in the symmetric ν_4, at the classical turning point the C_2H_2 is in a trans configuration; in the antisymmetric ν_5, it is in *cis*.
[g] Reference 18 calls the b_1 mode a "rock" and the b_2 mode a "wag."
[h] Reference 30.

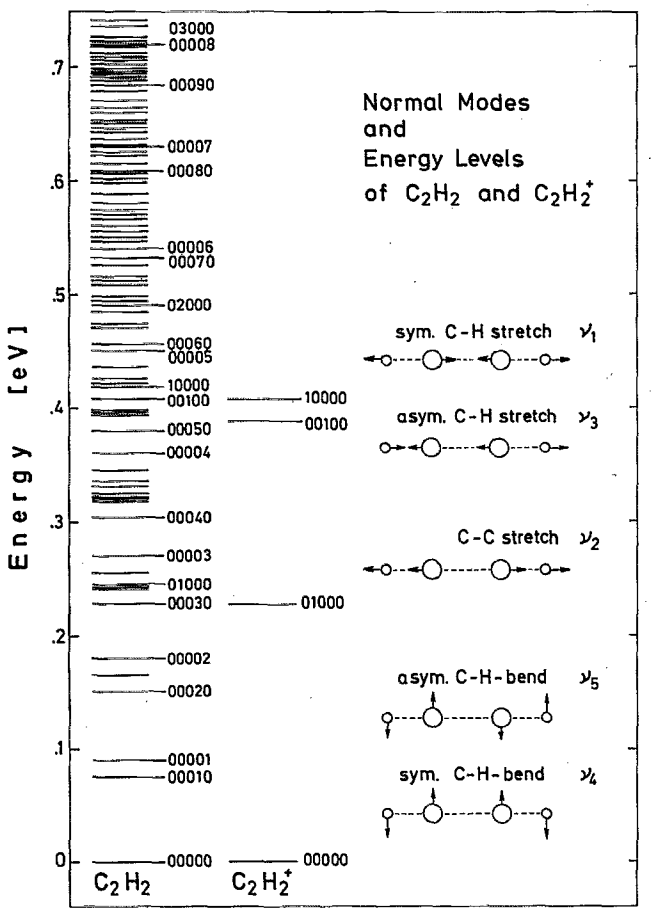

FIG. 1. Vibrational energy level diagram showing the vibrational fundamentals and overtones and combination levels in C_2H_2 assuming harmonic vibrations. The known levels of $C_2H_2^+$ are shown for comparison (Ref. 17). The motions corresponding to the different modes are also shown on the right.

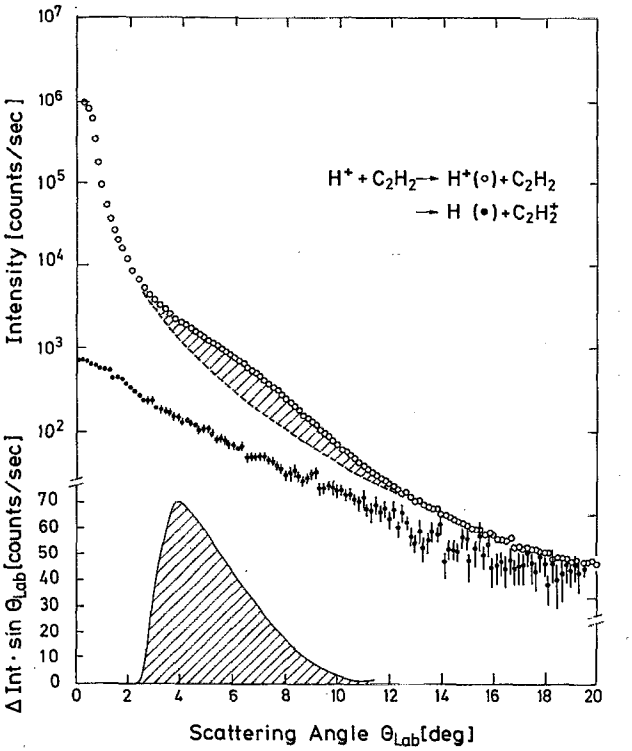

FIG. 2. Relative total differential cross sections for $H^+ + C_2H_2$ at $E = 30$ eV. The inelastic cross section (open circles) has a weak rainbow. The true position of the rainbow has been estimated by subtracting off the smooth background shown by the dashed line. To bring out the correct location of the rainbow the difference has been multiplied by $\sin\theta_{lab}$ and is shown on a linear scale at the bottom. The charge transfer cross section (filled dots), which is corrected for the lower H-atom detection probability, shows no rainbow. Between 2° and 14°, charge transfer is less probable than inelastic scattering by up to one order of magnitude. At large scattering angles, the probabilities of both processes become comparable.

III. EXPERIMENTAL RESULTS

The upper curve in Fig. 2 shows a log plot of the measured angular distributions of the intensities of the protons and the H atoms. These intensities are directly proportional to the differential total center-of-mass inelastic and charge transfer cross sections, respectively. Because of the favorable mass ratio the transformation from laboratory to center-of-mass frames has a negligible effect on the magnitude of the cross sections and the scattering angles in both cases.

The forward peak in the proton scattering distribution at $\theta < 2°$–$3°$ is largely due to the blast through of the unscattered incident beam and is spurious. To emphasize the structure in the angular distribution for proton scattering we have introduced a dashed line which provides a smooth interpolation between the small angle region ($\theta < 2°$) and the large angle region ($\theta > 12°$). The difference between this curve and the data points is attributed to a rainbow maximum resulting from a scattering extremum due to the focusing of protons by the potential well. This difference in intensities, multiplied by $\sin\theta$ to suppress the small angle region,[21] is plotted at the bottom of the figure. There it is seen that the maximum is in fact located at about 4°. The rainbow peak extends from about 3° to 8° and is roughly twice as broad as for H^+–Ne and Ar.[22] This large width is therefore probably due to a spread of well depths associated with the different relative orientations of the proton trajectory with respect to the molecular axis. The effective well depth ϵ can be estimated from this rainbow angle via the relation $\theta_R \approx 1.7\ \epsilon/E$, where E is the center-of-mass collision energy.[23] The factor 1.7 was found empirically to work better for ion–molecule interactions than the usual factor of about 2 for Lennard-Jones (12,6) potentials. In this way the effective well depth is estimated to be about 1.2 eV. It is interesting to note that this value is much smaller than the proton affinity of C_2H_2 which is well established as being 6.58 eV.[24] As will be discussed later the small value for the well depth probed by the proton is, in fact, related to an avoided crossing with a charge transfer channel.

The angular distributions of the charge exchange H-atom product, also shown in Fig. 2, have been multiplied by a factor of 20 to account for the lower H-atom detection efficiency.[4,20] From the ratio of the proton to H-atom signals in Fig. 2 the average probability of charge transfer out to

$\theta \sim 8°$ is about 10%. This is rather small when compared to transfer probabilities of 50% in CO_2 and N_2O (Ref. 8) and 70% in C_2H_4 (Ref. 25) in the same angular region. In CH_4, C_3H_8, and C_6H_6, at larger scattering angles the H-atom signals were even larger than the proton intensities implying that charge transfer is even more probable.[1,11] Above $\sim 8°$, well beyond the rainbow, the charge transfer probability in C_2H_2 does increase to nearly 50%. This suggests a stronger coupling between charge transfer and inelastic scattering which is more prevalent in repulsive collisions[4] than in small angle scattering, dominated by the attractive part of the potential.

Figure 3 shows some proton time-of-flight spectra converted to an energy loss scale[26] for scattering at $\Theta = 1°, 3°, 7°$, and 10°. All four spectra are dominated by the "elastic" peak which at $\Theta = 1°$ and to a lesser extent at 3° is due to "blast-through" of the unscattered intensity. A noticeable shift in the elastic peak to higher energy transfer which would be due to pure rotational excitation is not observed. This agrees with the fact that the rotational period of motion is at least two orders of magnitude larger than the collision time. Thus, with respect to rotational excitation the collision is within the Born approximation or sudden region, the energy spacing being even smaller ($B_e \simeq 0.14$ meV) than for O_2($B_e \simeq 0.27$ meV). Under these conditions the inelastic cross section is nearly proportional to the collision time[27] and accordingly strongly reduced in magnitude.

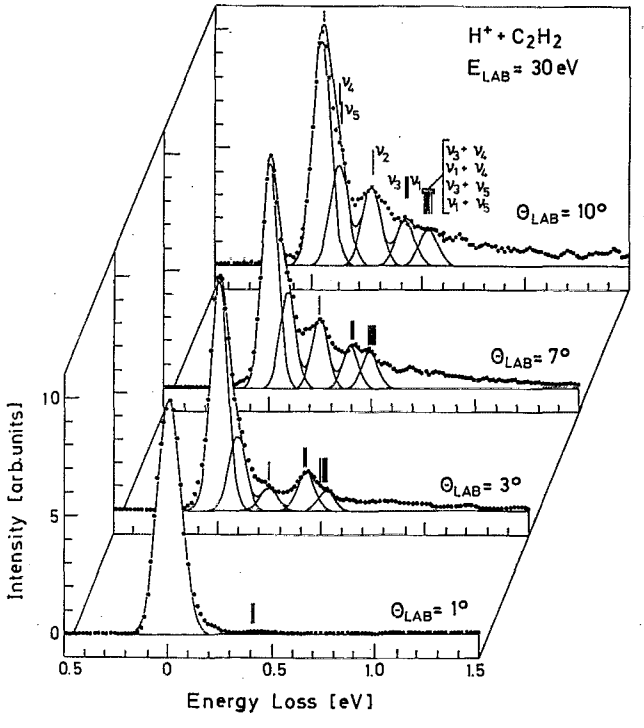

FIG. 3. Energy loss spectra for inelastic scattering of 30 eV H^+ from C_2H_2 at $\theta = 1°, 3°, 7°$, and 10°. The spectra have been fitted with Gaussian curves centered at the transition energies of the indicated vibrational modes. At $\theta = 3°$, the excitation of the C–H stretch modes (ν_1 or ν_3) dominate over the C–C stretch mode (ν_2), while at $\theta = 7°$ the relative probabilities are reversed.

The positions of the inelastic peaks in Fig. 3 can be assigned to the well-known acetylene vibrational modes listed in Table I. The two bending modes, ν_4 (76 meV) and ν_5 (90 meV), are too low in energy to be clearly separated from the elastic peak. Their presence has, however, been recently confirmed in preliminary measurements made in a new high resolution apparatus.[13] The first clearly resolved peak at 245 meV is attributed to the symmetric C–C stretch mode ν_2. The broader peak at 400 meV is assigned to the two C–H stretch modes, one of which is symmetric, ν_1 at 418 meV, and one antisymmetric, ν_3 at 408 meV, which are too close in energy to be resolved. Theoretical considerations, presented below, suggest that the excitation of ν_3 is more likely than ν_1. At about 500 meV there is some evidence for another peak which may correspond to a combination band of one of the bending modes ($\nu_{4,5}$) and one of the C–H stretch vibrations (ν_1, ν_3).

The unresolved monotonically decreasing tail at high energy losses is attributed to both overtone excitation of the above modes as well as combination bands. In this energy regime, the density of vibrational levels increases rapidly and no structure can be resolved. Preliminary high resolution measurements show in addition to the features seen here, overtones of ν_5, ν_3, and ν_1 and combination bands $\nu_2 + \nu_5$, $\nu_{3,1} + \nu_5$.[13]

Figure 4 shows time-of-flight spectra for H atoms produced in charge transfer collisions at three different scattering angles. Since the C_2H_2 molecule is not resonantly ionized it is interesting to compare the spectra with a photoelectron spectrum[28] which is also shown at the top of Fig. 3 for comparison. Due to the low H-atom detection efficiency the signal-to-noise ratio of the H-atom spectra is somewhat smaller than in Fig. 2. In these spectra there is also a problem with blast through of protons which undergo charge transfer in collisions with residual gas. This is most conspicuous at $\Theta = 0°$ where processes with resonant ($\Delta E \cong 0$) charge transfer have the largest cross sections and therefore predominate. All the measured H-atom spectra have an initial rise in intensity leading to a peak at $\Delta E = -2.2$ eV similar to that observed in the photoelectron spectrum. This observed acceleration of the H atoms compared to the protons is explained by the energy released resulting from the difference between the electron affinity of H^+ (13.6 eV) and the ionization potential of acetylene [11.4 eV (Ref. 29)]. Accordingly the peak at -2.2 eV corresponds to a complete conversion of electronic energy into translation energy with zero vibrational excitation of the molecular ion and therefore coincides with the threshold of ionization in the photoelectron spectrum. The observation of this strongly exothermic process, which is at variance with the energy resonance condition, is apparently favored by the Franck–Condon factors. In contrast to Fig. 3, the other vibrationally inelastic features are comparable in intensity with the vibrationally elastic scattering peak. This enhancement of vibrational excitation in charge transfer collisions is to be compared to the pure inelastic collisions shown in Fig. 3 and also with the photoelectron spectrum. It can be explained by the fact that these inelastic processes are more nearly resonant in energy. The low lying vibrations ν_4 and ν_5 cannot be resolved in the

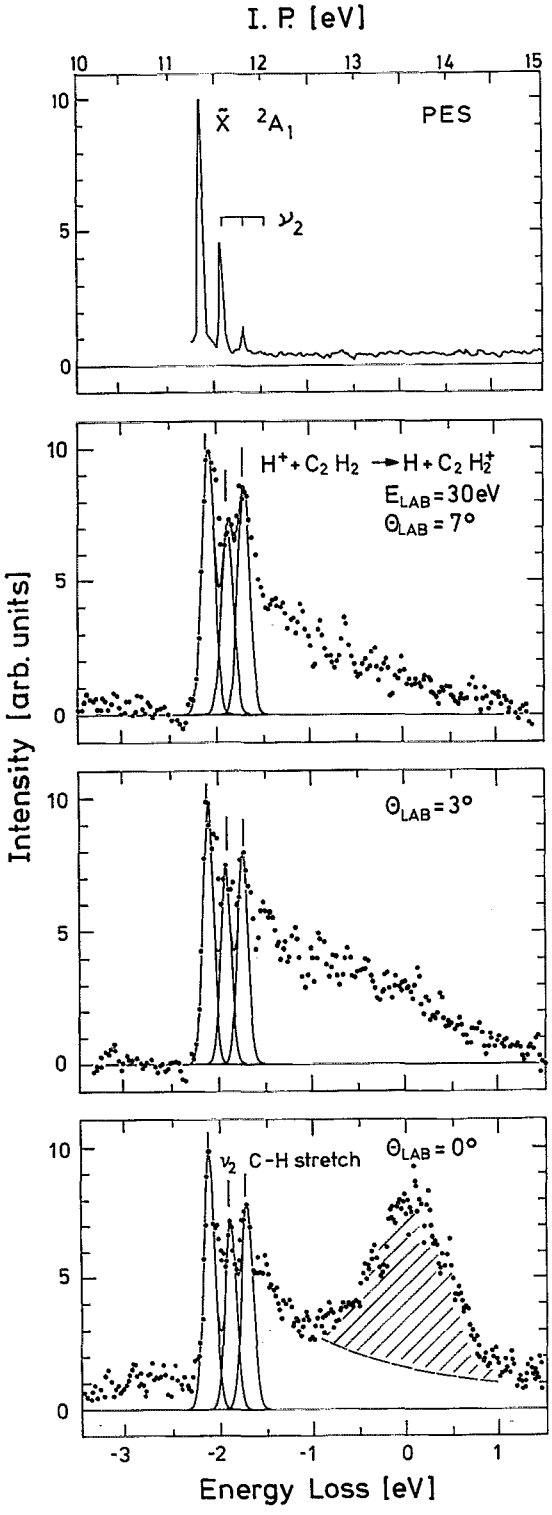

FIG. 4. Energy loss spectra of charge transfer in $H^+ + C_2H_2$ at 30 eV. Three spectra ($\theta = 0°$, 3°, and 7°) are shown, the lowest one being corrected for a background signal around $\Delta E = 0$ eV. The energy loss is measured with respect to the energy of the incident proton. For comparison a photoelectron spectrum (Ref. 28) is plotted at the top. All spectra show three peaks: at $\Delta E = -2.2$ eV, the "elastic" charge transfer, at $\Delta E = -1.97$ eV with excitation of the ν_2 mode, and a third peak near $\Delta E = -1.8$ eV which corresponds to charge transfer with excitation of an asymmetric C–H stretch of $C_2H_2^+$ (X^2A_1). In contrast to the inelastic proton spectra (Fig. 3) the distribution of vibrational peak intensities is nearly independent of angle.

charge transfer time-of-flight spectra. Since the degeneracy of these modes splits upon ionization, altogether four peaks are expected. Three have been measured in photoelectron spectroscopy at 62, 87, and 38 meV (Ref. 17) and are therefore well within the width of the elastic peak.

The first of the two resolved peaks corresponding to production of vibrationally excited $C_2H_2^+$ is assigned to the 227 meV symmetric C–C stretch mode ν_2 and coincides with the same feature observed in the photoionization spectrum. Note that this is the only mode that is observed in that spectrum. The second resolved peak is at 400 meV. Because the C–H bond lengths and bond strengths in C_2H_2 and $C_2H_2^+$ are quite similar (see below), the energy of C–H stretch vibrations should not change very much upon ionization. Therefore this feature is assigned to the ν_1 or ν_3 vibrations, both of which are C–H stretch modes. A mode at about this same energy has also been observed in a threshold photoelectron spectrum of acetylene,[17] and recently in an infrared spectrum of $C_2H_2^+$.[30]

No additional peaks are observed at higher energy transfers even though they would be favored by charge transfer resonance at $\Delta E \cong 0$ eV. This resonant effect was observed to lead to a strong enhancement of the corresponding transitions in CH_4,[1] H_2O,[9] and O_2.[2] Apparently in C_2H_2 the low Frank–Condon factors prevent these transitions from occurring. This inhibition of resonant charge transfer in C_2H_2 provides a possible explanation for the relatively small charge transfer total cross sections (Fig. 2).

Vibrational transition probabilities can be obtained from the relative heights of the peaks in the time-of-flight spectra in Figs. 3 and 4. Because the high-lying vibrational levels and overtones cannot be resolved, only relative probabilities normalized to the height of the elastic scattering peak rather than absolute probabilities (relative to all transitions) can be derived. Since the intensities in the high energy transfer tails are rather low, it is expected, however, that the correction due to transitions with greater energy transfer will be small. The results for both the CT and IS channels are shown in Fig. 5 as a function of scattering angle. The antisymmetric ν_3 and symmetric ν_1 modes are grouped together under "C–H stretch" and ν_4 and ν_5 under "bending" modes. For charge transfer, only the probabilities of C–C and C–H stretch excitation are available.

As shown in Fig. 5 these relative excitation probabilities of $C_2H_2^+$ are much greater than those of neutral C_2H_2. Relative to the elastic peak they are more than twice as large as for C_2H_2. Vibrational excitation of the C–H modes is more probable than of the C–C modes and the relative probabilities are nearly constant with respect to scattering angle, although a slight downward tendency in the ratio can be discerned. Due to the very small signal no reliable estimates of $C_2H_2^+$ vibrational excitation probabilities can be made for scattering angles larger than $\Theta = 9°$.

All of the four curves for vibrational excitation of neutral C_2H_2 show a steep increase at small and large angles and remain nearly constant at intermediate angles. This is consistent with the two scattering regions suggested by the angular distribution of Fig. 2: (1) the long range attractive region beyond the potential well, $\Theta < 4°$ and (2) the well

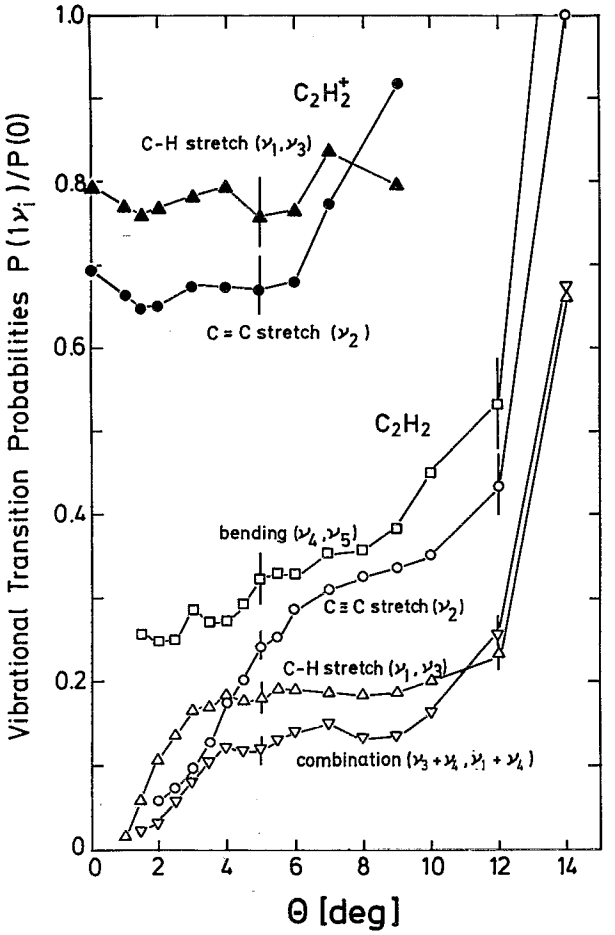

FIG. 5. Vibrational transition probabilities normalized to the height of the elastic peak derived for C_2H_2 and $C_2H_2^+$ for inelastic scattering (open symbols) and charge transfer (closed symbols). The excitation probabilities of C_2H_2 increase with angle, whereas for $C_2H_2^+$ they are nearly independent of angle up to about 6°.

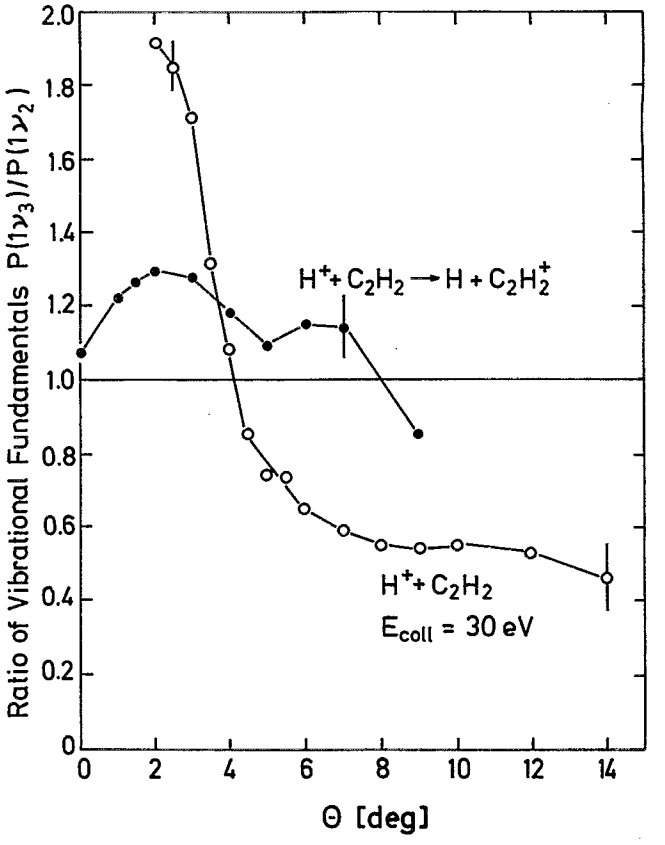

FIG. 6. Ratio of the probabilities for C–H to C–C stretch vibrations in C_2H_2 and $C_2H_2^+$. For neutral C_2H_2, the infrared active C–H stretch mode ν_3 dominates at small scattering angles, while the infrared inactive C–C stretch mode ν_2 dominates at large scattering angles. For $C_2H_2^+$, the ratio of ν_3 to ν_2 stays nearly constant at all angles.

region, $3 < \Theta < 8°$. In addition, the energy transfers in Fig. 5 suggest that there is a third region, $\Theta > 10°$. This region is attributed to hard repulsive interactions. In these close trajectories the much stronger coupling leads to a sharp increase in inelasticity. The excitation of the bending mode is the most probable process of all θ and appears to be related to the increasing influence of repulsive interactions. It is also interesting to observe that the C–C stretch vibrations become more probable than C–H stretch excitation just at the rainbow angle at 4°.

Figure 6 shows the ratios of the probability of C–H stretch excitation to that of C–C stretch excitation as a function of scattering angle for C_2H_2 and $C_2H_2^+$. For inelastic scattering there is a pronounced angular dependence. Below about the rainbow angle at $\theta = 4°$, the C–H excitation dominates the C–C excitation by nearly a factor of 2. This is the region where only the long range attractive potential is effective. At angles larger than $\theta = 6°$ where repulsive forces become important, the situation is nearly exactly reversed with C–C excitation consistently more probable than C–H excitation, also by a factor of 2. In the rainbow transition region $\theta = 3°$–8°, the probability ratio decreases very steeply.

This switchover between C–H stretch and C–C stretch vibrations at the rainbow angle is one of the most interesting observations of the present experiments. This is the first observation of the relative importance of the excitation of "peripheral" modes, e.g., C–H stretch vibrations, with which the projectile interacts directly, compared to " inner" modes, e.g., the C–C stretch vibrations, with which the projectile interacts only indirectly. Our results indicate what one intuitively would expect. Despite their higher frequencies and energy transfer the peripheral modes are excited in long range grazing collisions, whereas the softer inner C–C stretch vibrations can only be excited by an impulsive interaction involving presumably an entire CH unit. With increasing scattering angle and increasing impulsive nature of the collision an increasing fraction of the energy transferred finds its way into the inner part of the molecule.

By integrating over the observed energy loss distributions, the first moment of the distribution of energy loss to all internal degrees of freedom can be determined,

$$\langle \Delta E(\theta) \rangle = \int P(\Delta E,\theta) \cdot d\Delta E, \quad (3)$$

where $P(\Delta E,\theta)$ is the normalized measured energy loss distribution. $\langle \Delta E(\theta) \rangle$ is sometimes referred to as the average energy transfer. For charge transfer collisions the charge transfer exoergicity of -2.2 eV has been subtracted to obtain the net *internal* energy transfer. The results for both channels are displayed in Fig. 7. As expected the average internal energy transfer to the neutral C_2H_2 molecule is zero in the forward direction and rises monotonically with scattering angle. The plateau at $\theta \gtrsim 3.5°$ is related to the onset of the broad rainbow maximum in the angular distribution of Fig. 2 marking the onset of the transition from a predominantly attractive potential to a repulsive potential. This behavior has been predicted in classical trajectory calculations[12] which predict the plateau to begin at an angle corresponding to the rainbow angle. This criterion also yields a value of about 1 eV for the effective well depth. The second sharp rise sets in with the complete disappearance of the rainbow at about 8°. Here it appears that all the collisions are influenced by the strong repulsive forces. As expected, there is a strong similarity in the behavior in Fig. 5 and Fig. 7. The energy transfer to $C_2H_2^+$ ions, also shown in Fig. 7, does not show the same increase with θ but rather remains nearly constant. Similar behavior was observed for other molecules, CH_4,[1] C_2H_4,[25] C_3H_8, CH_3OH, C_6H_6 (Ref. 11) which was attributed to the energy resonance which favors significant excitation to occur even in soft $\theta = 0°$ collisions.

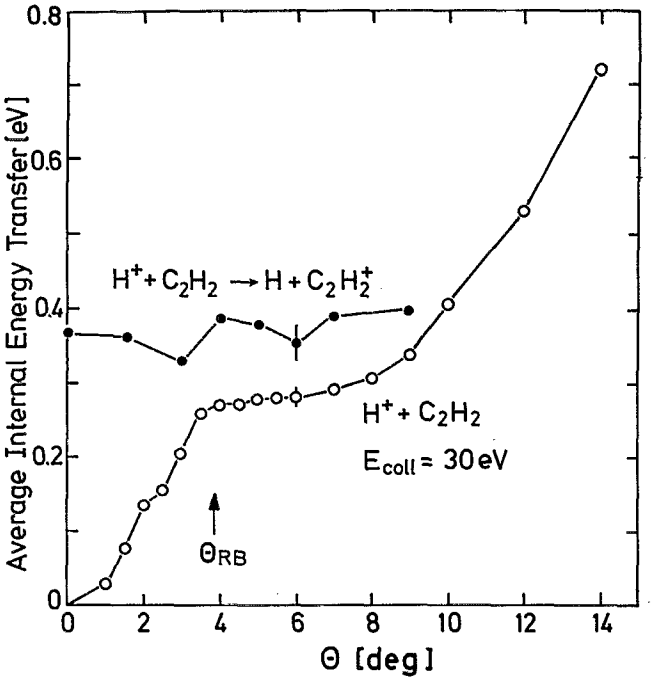

FIG. 7. Average internal energy transfer for inelastic scattering (open circles), and charge transfer (filled dots) as a function of scattering angles. Whereas the average amount of energy transfer in inelastic scattering increases towards larger angles, the values in charge transfer remain nearly constant. The shape of the inelastic curve shows a plateau between $\theta = 4°$ and 10° that is typical for systems that can be described by the forced oscillator mechanism (Ref. 12).

It was not possible to obtain data beyond 9° to determine if an increase in energy transfer occurs as the repulsive forces dominate the interaction, which would indicate the onset of an impulsive mechanism.

It should be noted that for both the IS and CT channels the average vibrational energy transfer is rather small, corresponding to less than one quantum of C–H stretch. In collisions of H^+ with other hydrocarbons,[11] the average amount of vibrational excitation is on the order of *several* C–H stretch quanta. For example, in inelastic scattering in $H^+ + C_2H_4$, the average internal energy transfer is three times higher than that observed here[25] and in $H^+ + CH_4$ the inelastic proton spectra show vibrational excitation with an energy transfer which goes beyond the dissociation limit of 4.4 eV.[1] The small amount of inelastic scattering in the $H^+ + C_2H_2$ system is thus rather striking. This difference may be related to the small probability for charge transfer. In CH_4 a substantial part of the inelastic scattering is attributed to collisions via an intermediate charge transfer state. Thus, the small probability for the formation of such an intermediate charge transfer state affects the inelasticity in the IS channel.

IV. DYNAMICAL APPROXIMATIONS

In view of the relative simplicity of the H^+–C_2H_2 system and the availability of parts of the potential hypersurfaces for $C_2H_3^+$, a theoretical description of at least some of the above observations would appear to be within reach. Unfortunately, as discussed in connection with our previous work on $H^+ + CH_4$,[1] a detailed realistic dynamical theory is completely out of the question at the present time. The calculation of a complete potential energy hypersurface for this system requires a total energy calculation as a function of all $3n - 6 = 9$ dimensions of the relative motions. To account for charge transfer the nonadiabatic coupling matrix elements must also be calculated. The problem is even more complicated since in view of the low mass of the proton a quantum mechanical scattering calculation is highly desirable. This is suggested by the fact that a recent IOS calculation of vibrationally resolved energy transfer in $H^+ + H_2$ (Ref. 7) gave better agreement with experiment than a classical trajectory surface hopping calculation.[5] Thus we conclude that similar calculations for systems with more than three nuclei are presently not possible. For this reason we have to resort to a number of drastic approximations in order to lay the basis for a semiquantitative description of the scattering dynamics.

To describe the $H^+ \cdots C_2H_2$ collisions we first simplify the dynamics by introducing the concept of a "direction of approach" as discussed previously.[1,12] This is illustrated in Fig. 8. For the grazing collisions of interest the trajectories can be approximated by straight lines with impact parameters of about several Ångstroms. Since the collision time $t = 2$ Å$/v_{proton}$ is on the order of 10^{-15} s, and therefore much shorter than the time of rotation, the molecules can be assumed to be stationary during the collision. The electric field pulse seen by the molecule at its center is shown at the bottom of Fig. 8. It consists of a component along y, perpen-

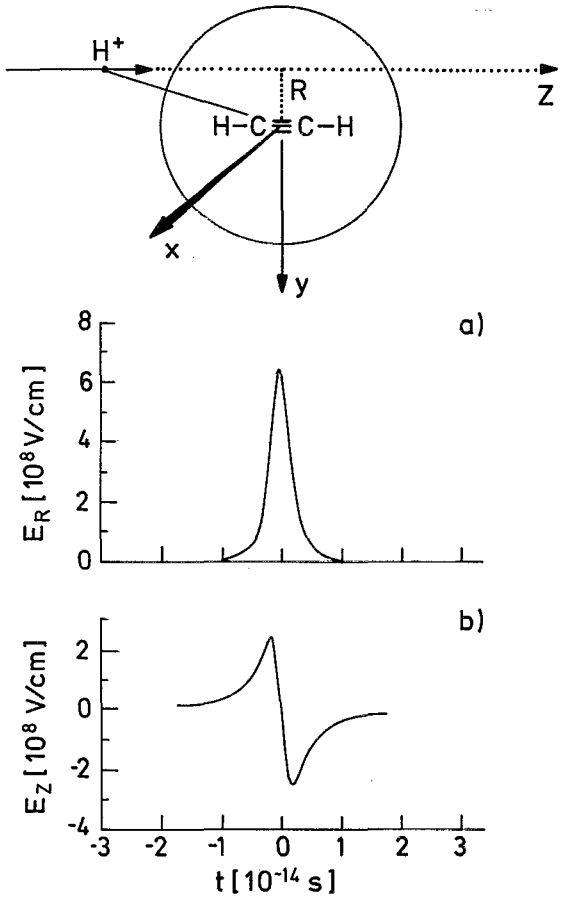

FIG. 8. Typical trajectories (a) and electric field strengths as a function of time (b). In the collision geometry illustrated in (a) the trajectory has been arbitrarily chosen to be parallel to the axis of the molecule. The direction of approach R is the direction perpendicular to the trajectory at the point of closest approach. The collision geometry in this example is therefore C_{2v}^{y}. The field strength along this direction is greater than that along the z direction. In the z direction the field strength is first positive and then negative and the two parts cancel when averaged over the time of the collision.

dicular to the trajectory, which produces an electric field on the order of 10^8 V/cm at the classical turning point.[12] The z component, parallel to the trajectory, is considerably smaller and is, in fact, zero at the classical turning point. For simplicity we neglect the parallel component and denote the reaction coordinate R as the direction of approach, which is along the y direction. Neglect of the parallel field component can be justified by recalling that the collision time is shorter than the vibrational period. Since the parallel field components are of equal magnitude but opposite in direction the energy transfer from the parallel component is about 50% smaller than from the perpendicular component.[12] Within this approximation the scattering problem is reduced to that of a central collision.

In Appendix A we provide a brief summary of the adaptation of time independent scattering theory to the remaining dynamical problem. The wave function is expanded in an adiabatic basis set where ϕ and χ denote the electronic and vibrational wave functions, respectively. Since this problem is still too difficult to solve we will use a procedure that is similar to that adopted in our earlier paper.[1] Our approach will be based on an examination of the coupling term $\tau'_{ij}(R)\partial/\partial R$ in Eq. (A3) in order to reestablish the propensity for the excitation of a given normal mode of the molecule. In particular, we will take advantage of symmetry considerations which require that the vibrational and electronic wave functions in Eq. (A2) satisfy certain conditions in order for the matrix elements not to vanish.

We emphasize that our discussion will only deal with symmetry selection rules which allows us to predict which of the modes are excited. The probabilities of the symmetry allowed transitions will depend on a number of factors including the magnitude of the potential gradients $\partial U/\partial R$, the gradients in the electronic wave functions $\partial/\partial R$ and on the Franck–Condon factors. The latter can be best estimated from the photoelectron spectra (see Fig. 4).

The coupling term $\tau'_{ij}(R)\partial/\partial R$ and the corresponding term $\tau'_{ij}(Q)\partial/\partial Q$ may be estimated from first-order perturbation theory[31]

$$\tau'_{ij}(R)\frac{\partial}{\partial R}=\frac{\hbar^2}{M}\frac{\langle\phi_j\chi_j|\partial U(q,Q)/\partial R\,|\phi_i\chi_i\rangle}{E_j(R)-E_i(R)}\frac{\partial}{\partial R} \tag{4}$$

and analogously for $\tau'_{ij}(Q)$. Q is one of the internal normal mode coordinates of the target molecule.

In the limit that $E_j(R)-E_i(R)$ is large the coupling term will go to zero and the vibronic coupling will have no effect. Then the solution of Eq. (A3) corresponds to the customary close coupling problem for scattering from a single potential surface.[32] In this case we do not have to invoke the central collision approximation since for small scattering angles the scattering problem can be simply approximated using a semiclassical approximation with a straight line trajectory.[12] The symmetry of the gradient $\partial U/\partial R$ of the interaction potential $U(R,Q)$ will determine which of the normal modes are excited.[14] Thus for the predominant ion-induced dipole interaction only the infrared active modes with the same symmetry as $\partial U/\partial R$ are affected. This mechanism has been designated the induced dipole mechanism (IDM).[1] For coupling via the polarizability and quadrupole moment gradients the Raman active and quadrupole derivative modes are excited.[14]

At the other extreme when the $E_j(R)-E_i(R)$ term in Eq. (4) is small, the nonadiabatic vibronic coupling matrix element is larger and will contribute. For the integral in the numerator to be nonzero, however, certain symmetry requirements have to be met. Let Γ denote the irreducible representations of the electronic wave functions ϕ_i, ϕ_j, the vibrational wave functions χ_{in}, χ_{jm} and of the vibrational wave function χ' along the reaction coordinate. Then the direct product of the Γ's satisfies the condition

$$\Gamma(\phi_j)\times\Gamma(\chi_{jm})\times\Gamma(\phi_i)\times\prod_n\Gamma(\chi_{in})\subset\Gamma(\chi'). \tag{5}$$

Note that we have now redefined the collective internal nuclear wave functions χ of the Appendix to be the individual normal mode wave functions with the indices m and n.

To solve Eq. (5) we recall that $\Pi_n \Gamma(\chi_{in})$ is always totally symmetric since it is the product of the irreducible representations of all the zero point vibrational normal modes before scattering.[33] The interacting states i and j are known in the present case so that the $\Gamma(\phi_i)$ and $\Gamma(\phi_j)$ are also known. $\Gamma(\chi')$ we define by selecting the direction of approach. Thus, from Eq. (5) we can establish which vibrational normal modes χ_{jm} can be coupled to the ground state.

Another way of stating the above selection rule is that only those vibrations of the molecule that conserve the total vibronic symmetry of the collision complex will be excited. The coupling between the surfaces leading to vibrational excitation in the target can be seen as its response to being thrust into an "unnatural" point group induced by the presence of the proton. Since the selection rule applies to the symmetries of the vibronic levels of the target molecule this mechanism is called the internal vibronic mechanism (IVM).[1]

In close collisions it is useful to introduce the concept of a quasimolecular complex. Even though the collision period is less than the vibrational period of the complex, the electronic states will generate forces which can influence the dynamics. These may be easier to envision when one describes the system not in terms of scattering, but rather as a unimolecular decomposition of the quasimolecule. The structure of the quasimolecule determines the collision geometry. Moreover, in this way we can utilize what is known about the electronic states of the protonated species. These states will interact most strongly in the vicinity of surface crossings and these interactions will determine the energy distribution in the separated products. To simplify the following discussion, we will switch to diabatic potential energy surfaces. (For a thorough discussion of the transformations required see Ref. 34.) The couplings thus occur at intersections, where the vibronic surfaces are degenerate.

These points of degeneracy can be classified into two groups: essential Jahn–Teller intersections and accidental conical intersections.[35,36] In the former, the electronic state symmetries are the same and we invoke the Jahn–Teller theorem which states that any nonlinear complex occupying a degenerate electronic energy level is unstable against a distortion which removes the degeneracy in first order. We assume that this distortion leads asymptotically to the scattering products. Thus, the coordinate along which distortion occurs becomes the effective reaction coordinate.

The energy shift accompanying the distortion is given by the first-order Jahn–Teller energy

$$\Delta E_m^{(1)} = \langle \phi_i \zeta_i | \frac{\partial U}{\partial Q_m} | \phi_i \zeta_i \rangle Q_m, \tag{6}$$

where the ζ_i denote the collective vibrational wave function of all the normal modes of the entire complex and Q_m is a given normal mode coordinate. We emphasize that we now no longer distinguish between R and Q.

Similar symmetry conditions for the nonvanishing of the coupling hold here as well.[37,38] This symmetry condition can be written

$$\Gamma(\phi_i) \times \Gamma(\phi_i) \subset \Gamma(\zeta_{im}), \tag{7a}$$

where ζ_{im} is the wave function of the mth normal mode in the ith electronic state and is only a function of Q_m. Thus the reaction coordinate (or coordinates) becomes that normal mode that satisfied Eq. (7a): A distortion along Q_m will lower the energy of the entire system.

In the latter case of conical intersections at points of accidental degeneracies, the electronic symmetries of the states involved may be different, but coupling occurs because the *vibronic* symmetries are the same and the symmetry condition

$$\Gamma(\phi_i) \times \Gamma(\phi_i) \subset \Gamma(\zeta_{jm}) \tag{7b}$$

holds. This coupling occurs through second-order, or pseudo Jahn–Teller effects between vibronic surfaces that at their asymptotes may be as much as 10–15 eV apart. This effect is particularly pronounced when strongly bonding or antibonding orbitals are involved.[39] The second-order energy shift is given by

$$\Delta E_m^{(2)} = \sum_j \left[|\langle \phi_i \zeta_i | \frac{\partial U}{\partial Q_m} | \phi_j \zeta_j \rangle Q_m|^2 \Big/ [E_i(Q) - E_j(Q)] \right]. \tag{8}$$

This "chemically induced pseudo Jahn–Teller" mechanism has been designated the quasi-molecular mechanism (QMM)[1] and has been thoroughly studied by Chiu[40] for $H^+ + CH_4$ and C_2H_2 collisions.

Note that these mechanisms and IVM should give the same results, since in principle, only the coordinate system has been transformed. That is, the symmetry condition of Eq. (7) is identical to Eq. (5) if the motion along R is included within the normal modes of the complex, and the "$\Pi_n \Gamma(\chi_{in})$" term is dropped since it is equal to unity.

V. THE POTENTIAL HYPERSURFACE

Figure 9 shows the general features of the potential hypersurfaces for two collision geometries, C_{2v}^v and C_s, with the yz plane taken as the collision plane. These geometries show the major features of the H^+–C_2H_2 potential energy surfaces which lead to stable $C_2H_3^+$ isomers. Note that the symmetry representations used in Fig. 9 are for the entire $[H \cdots C_2H_2]^+$ system. In order to translate these designations into those for the isolated acetylene or acetylene ion, the reader is referred to Table II. In the first column of Table II we show the irreducible representations in the $D_{\infty h}$ point group, which is the point group usually used to describe the ground state acetylene molecule and ion. The correlations in this table can be obtained from the character tables in a standard text on group theory such as Ref. 33.

The positions of the ground state minima and avoided crossings for the C_s orientation were estimated from the potential energy surfaces calculated for the nearly isoelectronic O_2H^+ system.[41(a)] These for the C_{2v}^y geometry were recently obtained in a very extensive, *ab initio* calculation of the full surface.[41(b)] The abscissa in Fig. 9 has been taken as the distance between the H^+ and one of the C atoms. The

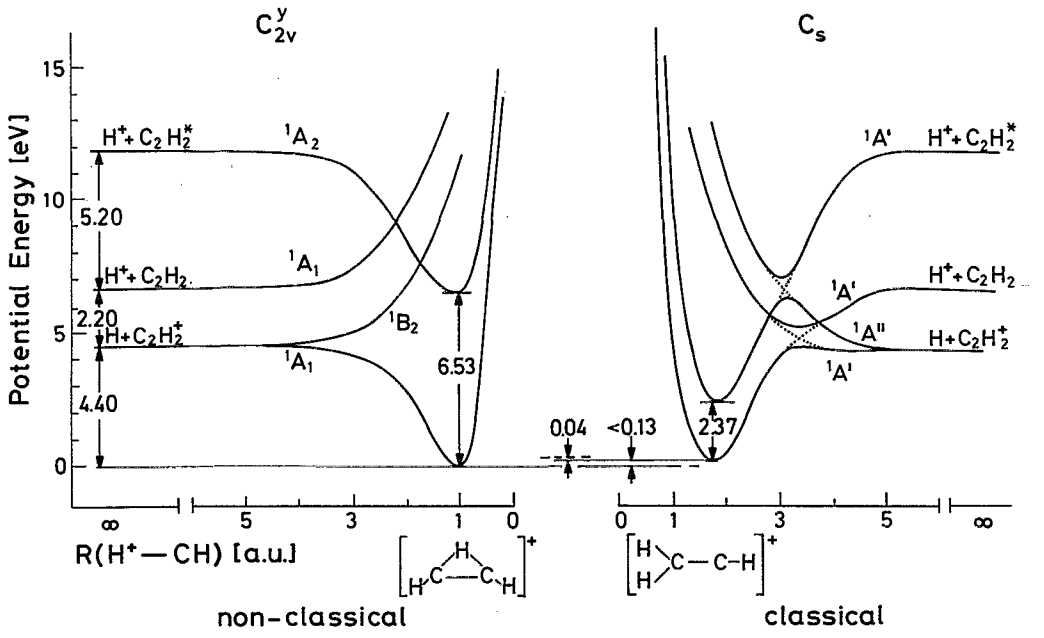

FIG. 9. Adiabatic potential energy curves of $(H + C_2H_2)^+$. The abscissa is the H^+ to C atom separation in atomic units (1 a.u. = 0.529 Å). The C_s curves are adapted from the calculations for the O_2H^+ surfaces [Ref. 41(a)], while the C_{2v}^y curves are taken from recent MRD-CI calculations [Ref. 41(b)]. The full lines are meant to be qualitative representations of the curves. The proton affinity is taken from the experimental data in Ref. 24, the charge transfer energetics from Ref. 42, and the acetylene electronic excitation energy from Ref. 29. The vertical excitation energies of the $C_2H_3^+$ complexes are taken from Ref. 43. The barrier height and energy separation between the two $C_2H_3^+$ structures is still a topic of discussion. By most accounts, the bridged structure is more stable by $\cong$0.13 eV and the barrier is $\simeq$0.04 eV [Refs. 44 and 41 (b)]. Note that the state designations for $H^+ + C_2H_2$, C_2H_2, and $H + C_2H_2^+$, $^1A_1$, $^1B_1$, and $^1B_2/^1A_1$, and $^1A'$, $^1A''$, are their symmetry representations in the C_{2v}^y and C_2 point groups, respectively. The usual state designations are, of course, $^1\Sigma_g^+$, ^1A_u, and $^1\Pi_u + {}^2S$ in the C_{2h} and $D_{\infty h}$ point groups, see Table II. The results of structure calculations on the equilibrium geometries are presented in Fig. 10.

TABLE II. Correlation between irreducible representations (i.e., molecular orbital and vibrational mode symmetries) of the point groups of C_2H_2 ($C_2H_2^+$) and $C_2H_3^+$.

C_2H_2 ($C_2H_2^+$) $D_{\infty h}$	$C_2H_3^+$
	C_{2v}^y (nonclassical)
σ_g^+, π_{uy}	a_1
σ_u^-, π_{gx}	a_2
σ_u^+, π_{gy}	b_1
σ_g^-, π_{ux}	b_2
	C_s (in-plane)
$\sigma_g^\pm, \sigma_u^\pm, \pi_{gy}, \pi_{uy}$	a'
π_{gx}, π_{ux}	a''
	C_{2v}^z (classical)
σ_g^+, σ_u^+	a_1
σ_g^-, σ_u^-	a_2
π_{gy}, π_{uy}	b_1
π_{gx}, π_{ux}	b_2
	$C_{\infty v}$ (collinear)
$\sigma_{g,u}^+$	σ^+ (A_1)
$\sigma_{g,u}^-$	σ^- (A_2)
$\pi_{g,u}$	π (E_1)

minima in the excited state surfaces are taken from the calculations of the geometries of $C_2H_3^+$: the equilibrium $(H\cdots C_2H_2)^+$ length increases by 3% in C_{2v}^y symmetry and decreases by 0.3% in C_s over those in the ground states.[19] The energetics are taken from various sources, all of which are referenced in the figure caption. Figure 10 shows the calculated equilibrium structures of both C_2H_2 and $C_2H_2^+$ as well as of the $C_2H_3^+$ complexes.

For both approaches in Fig. 9 the long range ion-induced dipole attraction in $H^+ + C_2H_2$ leads diabatically to a deep attractive well ($\cong$6.6 eV) in which the $C_2H_3^+$ complex is bound by the strong proton affinity. Whereas the C_{2v}^y approach leads to the nonclassical bridged $C_2H_3^+$ complex, approach through C_s leads to a collision complex resembling the other known stable structure of protonated acetylene, the classical vinyl cation of C_{2v}^z symmetry. The designations "classical" and "nonclassical" are the customary ones and of historical origin. Collinear $C_{\infty v}$ interactions should be repulsive, therefore, we have not included them in Fig. 9. The difference between the two $C_2H_3^+$ equilibrium conformations is between 40 and 130 meV[24,19] and the barrier to interconversion is of the same magnitude.[41] The H atoms in the complex can participate in a sort of merry-go-

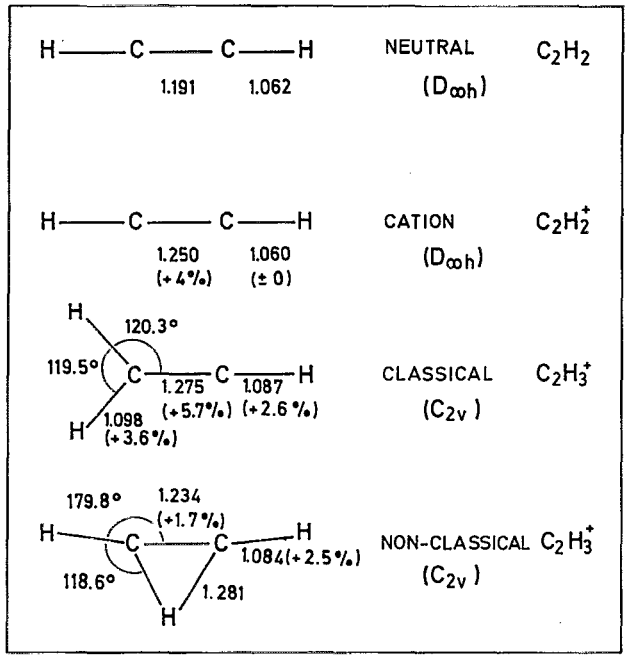

FIG. 10. Equilibrium structures of acetylene neutral and cation and of the protonated classical and nonclassical complexes. All percentage bond-length changes are referenced to neutral C_2H_2. Numerical values are from Ref. 19. Note that new photoelectron results (Ref. 17) suggest that the cation may not be linear as shown here.

round motion about the C–C bond.[40] The similarity in the potential well depths and well locations indicate that the interaction potential, at least in the well region, is actually quite isotropic.[41(b)] The perpendicular and parallel components of the polarizability of C_2H_2 which determine the long range potential anisotropy are $\alpha_\perp = 2.94$ and $\alpha_\parallel = 4.86$ Å^3.[45] The ratio of these values is not much larger than those for the "spherical" molecule H_2, $\alpha_\perp = 0.705$ Å^3 and $\alpha_\parallel = 1.007$ Å^3.[46] Thus, the lowest diabatic potential curves are rather isotropic both at large distances and also in the well region and the initial direction of approach should not be very important in determining the interaction. This is probably the reason why it has been possible to observe a rainbow in the proton angular distributions.

The other surfaces of interest are those for charge transfer, of which there are two for each collision geometry as discussed above. One leads to formation of $C_2H_2^+$ with an unpaired electron in the π_{uy} orbital and the other with it in the π_{ux} orbital. Because the polarizability of an H atom is small, the $H + C_2H_2^+$ surfaces are dominated by the repulsive parts. Only the state with the half-filled $C_2H_2^+$ π orbital in the collision plane couples with reactant surface and leads to an avoided crossing. As a result we predict a weak potential well of about 1–2 eV in the entrance channel for the C_s geometry only. This well depth correlates nicely with the observed rainbow in the proton angular distributions which was attributed to a well of 1.2 eV depth.

Unlike other hydrocarbon systems[1,10,11,25] there are no low-lying electronically excited states of $C_2H_2^+$ which may also couple to the reactant surface. This difference may also explain the inefficient charge and energy transfer observed in this system compared to other hydrocarbons. We have also indicated in Fig. 9 the estimated locations of the surfaces of the lowest excited states of C_2H_2 and $C_2H_3^+$. The experiments provide no evidence for the formation of $C_2H_2^*$ in the time-of-flight data, in agreement with previous experiments with $H^+ + Xe$ (Ref. 4) which have revealed that much higher collision energies are required for electronic excitation than are available in our experiment. However, through the QMM there is some probability that the distribution of vibrational states in the ground states of the scattered C_2H_2 and $C_2H_2^+$ products bears the stamp of distortion to the *trans* planar excited state.

No pronounced rainbow scattering is observed in the charge transfer process, which is consistent with the absence of a well in the outgoing part of the $H + C_2H_2^+$ potential for both orientations. The increased excitation at angles above 10° might be due to collisions off the repulsive wall of the $H + C_2H_2^+$ adiabatic potentials. Thus, the potential surfaces of Fig. 9 do account for the observations made in the angular distributions of this system.

VI. EXCITATION MECHANISMS

In this section we will consider in detail the three coupling mechanisms and how they apply to the proton–acetylene scattering system. IDM is expected to occur at all impact parameters since the collision trajectory always passes through the long range potential region. IVM is expected to become important in closer collisions where the energy difference between the potential energy surface decreases. QMM should be effective in very close collisions where the geometry of the collision complex at the turning point resembles that of the $C_2H_3^+$ molecular species.

For simplicity only three collision geometries, that is, three different reaction coordinates, along the y axis in C_{2v}, along the z axis in $C_{\infty v}$, and in the yz plane in C_s, are considered. In order to facilitate switching from one symmetry to another, the reader is referred to the correlations in Table II.

In inelastic excitation through IDM, those modes with large induced dipole moments along the reaction coordinate are favored. That is, as mentioned earlier, the symmetry of the gradient $\partial U/\partial R$ will determine which infrared modes will be affected. For example, in broadside C^v_{2v} attack, the C_2H_2 mode with the largest dipole moment with the same symmetry as R, which is a_1, is the C–H in-plane bend shown at the top of Fig. 11. According to the correlation in Table II and the data in Table I, in $D_{\infty h}$ symmetry this must correspond to the π_{uy} C–H bend of C_2H_2 which is the ν_5 mode. In collinear $C_{\infty v}$ attack, the reaction coordinate is again totally symmetric, a_1. Again checking Table II, we see that a_1 of $C_{\infty v}$ corresponds to $\sigma^+_{g,u}$ of $D_{\infty h}$. Table I shows two σ^+_g modes and one σ'_u mode. The former have no dipole moment and are thus inactive in this mechanism. That leaves ν_3, the antisymmetric C–H stretch as the only mode which will be excited in IDM in $C_{\infty v}$ approach. The right side of Fig. 11 illustrates this. Since C_s contains components corresponding to the above two situations, both ν_5 and ν_3 can be excited in these collisions. This is in agreement with the data of Fig. 5.

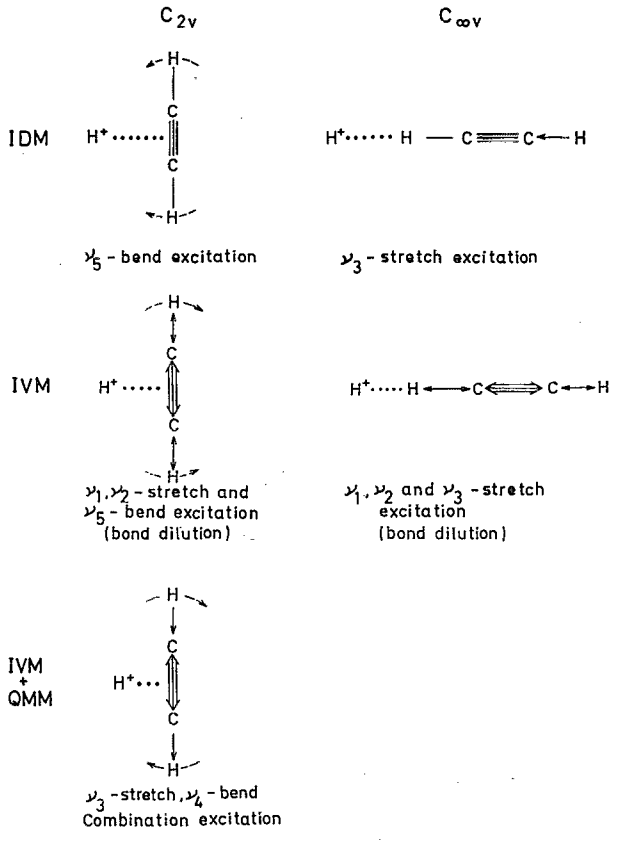

FIG. 11. In-plane vibrational modes excited in C_{2v}^{y} and $C_{\infty v}$ directions of approach in IDM, IVM, and QMM.

Below 4°, the most probable transition was attributed to an unresolved contribution from ν_4 and/or ν_5 and the second most probable to excitation of ν_1 and/or ν_3. The above considerations suggest that ν_1 and ν_4 make only minor contributions to these features.

At larger angles and smaller impact parameters the trajectories will come closer to the regions where the energetic spacing between the electronic states becomes smaller. This corresponds to the rainbow region $\theta > 3°$. The energetic closeness of states opens up the possibility of vibrational excitations via the IVM mechanism. When applying the selection rule for IVM, we have to consider the following electronic states. The reactant surface is A_1 in C_{2v}^{y} and $C_{\infty v}$, and A' in C_s symmetry. There are two product surfaces which are degenerate at $R = \infty$. At shorter H atom–acetylene ion separations, the one with the orbital containing the unpaired electron (left over after charge transfer) perpendicular to the collision plane is more repulsive than the product surface where the orbital containing the unpaired electron is in the collision plane. In C_{2v}^{y} symmetry, these two surfaces are $^1A_1$ and $^1B_2$; $^1B_2$ is more repulsive. In $C_{\infty v}$, these are $^1A_1$ and $^1A_2$ of which $^1A_2$ is the more repulsive, and in C_s they are $^1A'$ and $^1A''$ of which $^1A''$ is the more repulsive.

Thus, in C_{2v}^{y} approach the wave function in the reaction coordinate is totally symmetric $\Gamma(\chi') = A_1$. Using Eq. (5), for the first case we see that $\Gamma(\phi_i) = \Gamma(\phi_j) = \Pi_n \Gamma(\chi_{in}) = A_1$, so that, obviously $\Gamma(\chi_{jm}) = A_1$. For the second case, $\Gamma(\phi_i) = B_2, \Gamma(\phi_j) = A_1$, therefore $\Gamma(\chi_{jm}) = B_2$. In C_{2v}^{y} approach, therefore, IVM leads to excitation of acetylene modes of a_1 and b_2 symmetry. Looking at Table II we see that a_1 correlates to σ_g^+ and π_{uy} of $D_{\infty h}$. Inspecting Table I we see that the C_2H_2 and $C_2H_2^+$ modes of these symmetries are ν_1, ν_2, and ν_5. Similarly we find that the b_2 mode in C_{2v}^{y} also corresponds to ν_5.

Additionally, combinations of normal modes whose symmetry product is either a_1 or b_2 can be excited. For example, a combination of two a_1 modes, two b_1 modes, or a $b_1 + a_2$ band, which has b_2 symmetry, is allowed. The first case simply corresponds to a sum of ν_1, ν_2, and ν_5. For the second case we again look at Table II and see that b_1 symmetry in C_{2v}^{y} corresponds to σ_u^+, π_{gy} in $D_{\infty h}$. Table I shows that ν_3 has σ_u^+ symmetry and ν_4 corresponds to π_{gy}. Thus, a combination $\nu_3 + \nu_4$ can be expected. This suggests that the highest energy peak in Fig. 3, shown most clearly in the 10° data, is due to $\nu_1 + \nu_5$ and $\nu_3 + \nu_4$. Repeating this procedure for the $b_1 + a_2$ case shows that this, too, corresponds to $\nu_3 + \nu_4$, where now the out-of-plane π_{gx} component of ν_4, instead of the in-plane π_{gy}, participates. Other combinations are, of course, also possible, but these are the most interesting, as will be pointed out below. The in-plane component of the $\nu_3 + \nu_4$ combination band is also pictured in Fig. 11.

Repeating the procedure for $C_{\infty v}$ symmetry we find that since, again, $\Gamma(\chi')$ is the totally symmetric A_1, the product of the electronic energy state symmetries and the mode excited must also be A_1. Table II indicates that these modes correlate to $\sigma_{g,u}^+$ and $\sigma_{g,u}^-$ respectively. Table I lists only $\sigma_{g,u}^+$ modes, namely, ν_1, ν_2, ν_3.

In C_s geometry we find that the two interactions allow a' and a'' mode excitation, i.e., the low symmetry of this collision geometry allows all C_2H_2 and $C_2H_2^+$ modes to be excited.

Let us briefly consider the IVM mechanism qualitatively for the C_{2v}^{y} approach. In the case of mixing between the two A_1 surfaces, the a_1 vibrations ν_1, ν_2, ν_5 are excited. These modes are precisely those that one would expect to be affected upon (partial) removal of an electron from the π_{uy} orbital of acetylene: The C–C bond is stretched in ν_1 and ν_2 due to the proton withdrawing electron density and the ν_5 distortion aids in maximizing the proximity of the C–C HOMO to the proton. This is pictured in the middle section of Fig. 11 where we have drawn all of the a_1 modes together. This is thus consistent with the increase of C–C excitation (Figs. 5 and 6) and charge transfer (Fig. 2) in the general vicinity of the rainbow angle, which corresponds to the region of strong vibronic coupling at about 4.5 a.u. It is also consistent with the trends in bond lengths and angles in the calculations of the equilibrium structures shown in Fig. 10. Upon ionization the C–C bond is lengthened and in the complex the acetylenic H atoms are bent back away from the approaching proton.

Note that the $\nu_3 + \nu_4$ combination band (the $a_1 + b_1$ combination) is especially interesting since it correlates to the modes of the nonclassical complex (Table I). As shown at the bottom of Fig. 11, these modes look like those needed to distort to a species resembling the classical vinyl cation.

This is consistent with the prediction of a planar merry-go-round motion of H's about the C–C core and facile interconversion between the two equilibrium geometries.[40]

The $A_1 - B_2$ coupling which can result in excitation of the ν_5 π_{ux} must be small. Since we have constrained the proton approach to the *yz* plane, the removal of an electron from the π_{ux} orbital and concomitant excitation of a π_{ux} vibration, both lying in the *xz* plane, is unlikely.

As mentioned in the previous section, we can equivalently evaluate which vibrational modes should be excited by considering the diabatic surface of a dissociating quasimolecular complex. In addition to the coupling interactions predicted above, we must then include the effects of very high lying electronic states, i.e., the third excitation mechanism QMM.

The lowest excited state of acetylene is formed by promoting a bonding π_u electron to an antibonding π_g orbital. The molecule is planar with the H atoms in *trans* positions, that is, the positions of the nuclei are similar to those in acetylene undergoing a ν_4 symmetric bend. In the standard nomenclature this state is designated as ^1A_u of the C_{2h} point group where our *x* is the axis of highest symmetry. If we add a proton to such a structure, in the *yz* plane of the molecule at the center of the C–C bond, then in the C^y_{2v} point group representation this becomes a B_1 state. Approach in C_s in the *yz* plane produces a A' complex, as indicated in Fig. 9. No complex can form in $C_{\infty v}$.

Thus, according to the derived symmetry rules, second-order Jahn–Teller coupling of the reactant A_1 and excited state B_1 surfaces in C^y_{2v} will lead to excitation of b_1 modes, that is, ν_3 and/or ν_4. This is, of course, logical in view of the geometry of the excited state. In C_s approach, coupling of the ground and excited A' states leads to a' mode excitation, namely, σ_g^+, σ_u^+, π_{gy}, and π_{uy} (Table II). That is, all modes except for the *x* components of ν_4 and ν_5 will be affected (Table I).

The results of the above discussion are summarized in Table III where the theoretical mode propensities are compared with the experimental observations.

TABLE III. Comparison of vibrational modes observed experimentally with theoretical predictions for the different models in different scattering angle regions.

Scattering angles		Low θ	Intermediate θ	High θ
Expt.		ν_5 and/or ν_4 ν_3 and/or ν_1	ν_5 and/or ν_4 ν_2	All modes and combination bands
Theory				
	C^y_{2v}	ν_5		
IDM	$C_{\infty v}$	ν_3		
	C_s	ν_5/ν_3		
	C^y_{2v}		$\nu_1,\nu_2,\nu_5,$ $(\nu_3+\nu_4)$	
IVM	$C_{\infty v}$		...	
	C_s		All modes	
	C^y_{2v}			ν_3,ν_4
QMM	$C_{\infty v}$			...
	C_s			ν_1,ν_2,ν_3

VII. SUMMARY

We have shown that three mechanisms, one relying on the long range Coulombic interaction between the proton and molecule (IDM) and two on the vibronic interactions among the potential surfaces of the collision system (IVM, QMM), governed by simple symmetry selection rules, can adequately identify which vibronic states will be affected in a proton–molecule scattering process. These mechanisms also agree with the features of the potential energy surface inferred from the angular distribution data. In particular, the data suggest a potential well of about 1.2 eV which we attribute to an avoided crossing at which the IVM becomes important. Our models can explain the mechanism of excitation of the C–H and C–C stretches and the switchover in the relative probabilities between these as shown in Fig. 6. It should be noted that this is the first system in which such switching behavior has been observed. We can show that C–C stretch excitation occurs only in collisions which are close enough for vibronic coupling to occur, explaining the rise in ν_2 intensity at angles beyond the rainbow.

A more detailed analysis is required to understand the intensities of the observed transitions.

Another result shown in Fig. 5 which our symmetry scheme fails to address is why C–H excitation should be more probable than C–C excitation in the charge transfer process. For this, at least a knowledge of the Franck–Condon factors is necessary. Similarly, the simple theory cannot explain the result of Fig. 7 showing that the amount of energy transferred into the scattered product ion is higher than into the scattered product neutral. This behavior, which has been observed in all other systems studied,[11] appears to be related with the energy resonance condition which favors transitions for which the total energy transfer is as small as possible.

A final point of interest concerns the low efficiency of energy transfer in the inelastic and charge transfer channels in acetylene in comparison with other polyatomic hydrocarbons [CH_4,[1] C_2H_4, C_3H_8, CH_3OH, C_6H_6 (Ref. 11)]. This cannot be a result of collision geometry restrictions since the potential is expected to be sampled from all possible directions and appears to be rather isotropic. However, the MRD-CI calculations[41(b)] already show that one of the important directions of approach exhibits no curve crossing, thereby lowering the overall probability of the CT processes to occur. It still remains to be seen if the C_s geometry from actual calculations will confirm the qualitative guess of our Fig. 9 or will also show lack of curve crossing geometries.

ACKNOWLEDGMENTS

We are grateful to Dr. H. Köppel and Dr. H. D. Meyer (Heidelberg, Germany) N. Sathyamurthy (Kanpur, India) and F. Gianturco (Rome, Italy) for stimulating discussions

and useful suggestions. We are grateful to Dr. M. Noll for helpful advice on various experimental problems.

APPENDIX A

Neglecting rotations and spin–orbit interactions the Hamiltonian for the dynamical problem is[47,48]

$$H = H_{el} - \frac{\hbar^2}{2M}\frac{\partial^2}{\partial R^2} - \frac{\hbar^2}{2\mu}\frac{\partial^2}{\partial Q^2}, \tag{A1}$$

where

$$H_{el} = -\frac{\hbar^2}{2m_{el}}\sum_n \frac{\partial^2}{\partial q^2} + U(q,Q) + U(q,R)$$

is the electronic Hamiltonian for fixed positions of the nuclei. M and μ are the reduced masses of the complex and the target molecule and m_{el} is the electron mass. The electronic coordinates are denoted by q, while Q refers to the nuclear degrees of freedom in all the normal modes, and R is the reaction coordinate, which is the same as the direction of approach. H_{el} includes the kinetic energy of all n electrons and all the Coulomb (electron–electron, electron–nuclei, and nuclei–nuclei) energies denoted collectively by $U(q,Q)$ and $U(q,R)$.

The total wave function is expanded in terms of electronic wave functions ϕ_i in an adiabatic basis[49]

$$\psi(q,Q) = \sum_i c_i \phi_i(q,Q,R)\chi_i(Q,R)\chi_i'(Q,R), \tag{A2}$$

where the c_i are the mixing coefficients (for a well defined initial state, $c_i = 1$). The ϕ_i count for all the possible electronic states of the collision system, including the charge transfer states. They include a R^{-1} factor in order to remove first derivative terms from the Schrödinger equation.[48] The $\chi_i(Q,R)$ are the internal vibrational wave functions, which, typically, are a product of normal mode wave functions. The $\chi_i'(Q,R)$ is the nuclear wave function corresponding to relative motion along the reaction coordinate R. By appropriate transformations, the R's and Q's may be intermingled and combined to become the normal coordinates of the collision complex. Substituting Eq. (A2) into the Schrödinger equation, multiplying on the left by $\phi_j^*\chi_j^*$ and integrating over the coordinates q and Q we obtain a set of coupled differential equations in the electronically adiabatic basis,

$$c_j\left[-\frac{\hbar^2}{2\mu}\frac{\partial^2}{\partial Q^2} - \frac{\hbar^2}{2M}\frac{\partial^2}{\partial R^2} + E_j(R) - E\right]\chi_j'(R,Q) = \sum_{j\neq 1} c_i\left[\tau_{ij}'(R)\frac{\partial}{\partial R} + \tau_{ij}''(R) + \tau_{ij}'(Q)\frac{\partial}{\partial Q} + \tau_{ij}''(Q)\right]\chi_i'(R,Q), \tag{A3}$$

where we have neglected some diagonal Born–Oppenheimer terms which are small compared to the total vibronic energies $E_j(R)$ for the jth electronic state. $E_j(R)$ is defined by the effective Schrödinger equation[50]

$$\left(H_{el} - \frac{\hbar^2}{2\mu}\frac{\partial^2}{\partial Q^2}\right)\phi_j\chi_j = E_j(R)\phi_j\chi_j. \tag{A4}$$

The nonadiabatic coupling matrix elements are denoted by τ' and τ'' and are given by

$$\tau_{ij}'(R) = \frac{\hbar^2}{M}\left\langle \phi_j\chi_j \left| \frac{\partial}{\partial R} \right| \phi_i\chi_i \right\rangle, \tag{A5}$$

and

$$\tau_{ij}''(R) = \frac{\hbar^2}{2M}\left\langle \phi_j\chi_j \left| \frac{\partial^2}{\partial R^2} \right| \phi_i\chi_i \right\rangle. \tag{A6}$$

Similar expressions hold also for $\tau_{ij}'(Q)$ and $\tau_{ij}''(Q)$. The $\tau_{ij}'(R)$ and $\tau_{ij}''(R)$ account for the mixing of one vibronic state i with another state j as a result of the relative motion in the reaction coordinate R. The coupling matrix element $\tau_{ij}'(R)$ is velocity dependent since it involves $\partial/\partial R$ operating on the nuclear wave function χ_i. At the high velocity grazing collisions of interest here it represents the predominant coupling matrix element.[51] Finally we note that a parallel treatment leads to a similar set of coupled differential equations for $\chi_i'(R,Q)$ with $E_j(R)$ replaced by $E_i'(Q)$ and with χ and χ', R and Q interchanged.

In order to calculate the inelastic differential cross section it would be necessary to solve Eq. (A3) and match the solutions to the appropriate scattering boundary conditions. Such a procedure would require a calculation of the electronic wave functions and their gradients at every collision geometry in order to evaluate the matrix elements of Eqs. (A5) and (A6). Moreover, there are other formidable mathematical problems in solving these equations. These can be circumvented in some simple cases[34] but the problems inherent in a polyatomic system have not been addressed in detail.

[1] Y. N. Chiu, B. Friedrich, W. Maring, G. Niedner, M. Noll, and J. P. Toennies, J. Chem. Phys. **88**, 6814 (1988).
[2] M. Noll and J. P. Toennies, J. Chem. Phys. **85**, 3313 (1986).
[3] E. C. G. Stückelberg, Helv. Phys. Acta **5**, 369 (1969).
[4] M. Baer, R. Düren, B. Friedrich, G. Niedner, M. Noll, and J. P. Toennies, Phys. Rev. A **36**, 1063 (1987).
[5] G. Niedner, M. Noll. J. P. Toennies, and Ch. Schlier, J. Chem. Phys. **87**, 2685 (1987).
[6] M. Baer, G. Niedner, and J. P. Toennies, J. Chem. Phys. **88**, 1461 (1988).
[7] M. Baer, G. Niedner, and J. P. Toennies, J. Chem. Phys. **91**, 4169 (1989).
[8] G. Niedner, M. Noll, and J. P. Toennies, J. Chem. Phys. **87**, 2067 (1987).
[9] B. Friedrich, G. Niedner, M. Noll, and J. P. Toennies, J. Chem. Phys. **87**, 5256 (1987).
[10] U. Gierz, M. Noll, and J. P. Toennies, J. Chem. Phys. **82**, 217 (1985).
[11] G. Niedner, Dissertation, Georgia Augusta Universität Göttingen, Fed. Rep. Germany, 1988, Max-Planck-Institut für Strömungsforschung, Bericht 13/1988.
[12] U. Gierz, M. Noll, and J. P. Toennies, J. Chem. Phys. **83**, 2259 (1985).
[13] W. Maring, J. P. Toennies, R. G. Wang, and H. B. Levene, Chem. Phys. Lett. (in press).
[14] T. Ellenbroek and J. P. Toennies, Chem. Phys. **71**, 309 (1982).
[15] G. Herzberg, *Molecular Spectra and Molecular Structure*, Vol. III (Van Nostrand, New York, 1966).
[16] W. M. A. Smit, A. J. von Straten, and T. Visser, J. Mol. Struct. **48**, 177 (1978).
[17] R. Unwin, H. H. Rotermund, A. M. Bradshaw, and W. Peatman, Annual Report of the Berlin Synchrotron Facility (BESSY), 193 (1989).
[18] G. P. Raine and H. F. Schaefer III, J. Chem. Phys. **81**, 4034 (1984).
[19] T. J. Lee and H. F. Schaefer III, J. Chem. Phys. **85**, 3437 (1986).
[20] J. Ray, C. Barnett, and B. van Zyl, J. Appl. Phys. **83**, 2259 (1985).
[21] H. Pauly and J. P. Toennies, Methods Exp. Phys. **7A**, 227 (1968).
[22] F. A. Gianturco, G. Niedner, M. Noll, E. Semprini, F. Stefani, and J. P. Toennies, Z. Phys. D. **7**, 28 (1987).

[23] G. D. Barg, G. M. Kendall, and J. P. Toennies, Chem. Phys. **16**, 243 (1976).
[24] L. A. Curtiss and J. A. Pople, J. Chem. Phys. **88**, 7405 (1988).
[25] N. Aristov, W. Maring, G. Niedner, J. P. Toennies, Y.-N. Chiu, and H. Köppel, J. Chem. Phys. (submitted).
[26] M. Faubel and J. P. Toennies, Adv. At. Mol. Phys. **13**, 229 (1977).
[27] The collision time effect is most easily understood within the framework of the forced oscillator model energy transfer expression as discussed in Ref. 12.
[28] D. W. Turner, C. Baker, A. D. Baker, and C. R. Brundle, *Molecular Photoelectron Spectroscopy* (Wiley-Interscience, London, 1970).
[29] K. Kimura, S. Katsumata, Y. Achiba, T. Yamazaki, and S. Iwata, *Handbook of He I Photoelectron Spectra of Fundamental Organic Molecules* (Japan Scientific Societies, Tokyo, 1981).
[30] M. W. Crofton, M. F. Jagod, B. D. Rehfuss, and T. Oka, J. Chem. Phys. **86**, 3755 (1987).
[31] W. D. Hobey and A. D. McLachlan, J. Chem. Phys. **33**, 1695 (1960).
[32] W. R. Lester, Jr., Adv. Quantum Chem. **9**, 199 (1979).
[33] F. A. Cotton, *Chemical Applications of Group Theory* (Wiley-Interscience, New York, 1971).
[34] M. Baer, in Topics in Current Physics, Vol. 33, *Molecular Collision Dynamics*, edited by J. M. Bowman (Springer, Berlin, 1983), p. 118; *Theory of Chemical Reaction Dynamics* (CRC, Boca Raton, 1985).
[35] M. Desouter-Lecomte, C. Galloy, J. C. Lorquet, and M. Vaz Pires, J. Chem. Phys. **71**, 3661 (1979).
[36] H. C. Longuet-Higgins, Proc. R. Soc. London, Ser. A **344**, 147 (1975).
[37] R. G. Pearson, *Symmetry Rules for Chemical Reactions* (Wiley-Interscience, New York, 1976).
[38] L. D. Landau and E. M. Lifshitz, *Quantum Mechanics, Non-Relativistic Theory*, Vol. 3 of Course of Theoretical Physics (Pergamon, Oxford, 1965), 2nd revised edition, p. 380.
[39] I. B. Bersuker and V. Z. Polinger, *Vibronic Interaction in Molecules and Crystals*, Springer Ser. Chem. Phys. Vol. 49 (Springer, Heidelberg, 1989).
[40] Y. N. Chiu, J. Phys. Chem. **92**, 4352 (1988).
[41] (a) F. Schneider, L. Zülicke, F. DiGiacomo, F. A. Gianturco, I. Paidarova, and R. Polak, Chem. Phys. **128**, 311 (1988); D. Grimbert, B. Lassier Govers, and V. Sidis, *ibid.* **124**, 187 (1988); G. Winkelhofer, R. Janoschek, F. Fratev, and P. von Rague Schleyer, Croat. Chem. Acta **56**, 509 (1983); (b) F. A. Gianturco, A. Palma, and F. Schneider, Int. J. Quantum Chem. **37**, 729 (1990).
[42] A. A. Radzig and B. M. Smirnov, *Reference Data on Atoms, Molecules, and Ions* (Springer, Berlin-Heidelberg, 1985).
[43] J. Weber, U. Yoshimine, and A. D. McLean, J. Chem. Phys. **64**, 4159 (1976). These authors use a molecular coordinate system where the primary molecular axis is x rather than z. This reverses the b_1 and b_2 designations from the convention used in Ref. 33.
[44] J. Berkowitz, C. A. Mayhew, and B. Ruscic, J. Chem. Phys. **88**, 7396 (1988).
[45] G. N. Alms, A. K. Burnham, and W. H. Flygare, J. Chem. Phys. **63**, 332 (1975).
[46] E. A. Reinsch, J. Chem. Phys. **83**, 5785 (1985).
[47] J. C. Tully, in *Dynamics of Molecular Collisions, Part B.*, edited by W. H. Miller (Plenum, New York, 1976).
[48] M. S. Child, in *Atom-Molecule Collision Theory*, edited by R. B. Bernstein (Plenum, New York, 1979).
[49] This expansion is similar to that used in the usual dynamic treatment of vibronic coupling (Refs. 47 and 48).
[50] Reference 47, p. 433.
[51] Reference 47, p. 435.